Title
Effect of Crystallization on Proton Transport in Model Polymer Electrolyte Membranes

Journal
Macromolecules, 47(13)

ISSN
0024-9297

Authors
Beers, Keith M
Wong, David T
Jackson, Andrew J
et al.

Publication Date
2014-07-08

DOI
10.1021/ma500298w

Peer reviewed

Macromolecules

Article

pubs.acs.org/Macromolecules

Effect of Crystallization on Proton Transport in Model Polymer Electrolyte Membranes

Keith M. Beers,[†,‡,⊥] David T. Wong,[#,§,⊥] Andrew J. Jackson,[$,&,%,§] Xin Wang,[§] John A. Pople,[@] Alexander Hexemer,[∥] and Nitash P. Balsara*[,§,‡,⊥]

[†]Exponent, 149 Commonwealth Drive, Menlo Park, California 94025, United States

[‡]Materials Sciences Division, [§]Environmental Energy Technologies Division, and [∥]Advanced Light Source, Lawrence Berkeley National Laboratory, Berkeley, California 94720, United States

[⊥]Department of Chemical and Biomolecular Engineering, University of California, Berkeley, Berkeley, California 94720, United States

[#]Exponent, 9 Strathmore Road, Natick, Massachusetts 01760, United States

[$]European Spallation Source ESS AB, P.O. Box 176, 221-00 Lund, Sweden

[&]Department of Chemical Engineering, University of Delaware, 150 Academy St., Newark, Delaware 19716, United States

[%]NIST Center for Neutron Research, 100 Bureau Drive, Gaithersburg, Maryland 20899, United States

[@]Stanford Synchrotron Radiation Laboratory, Menlo Park, California 94025, United States

ABSTRACT: Polymer electrolyte membranes with bicontinuous microphases comprising soft hydrated domains and mechanically robust hydrophobic domains are used in a wide range of electrochemical devices including fuel cells and electrolyzers. The self-assembly, water uptake, and proton conductivity of model block copolymer electrolytes with semicrystalline hydrophobic blocks were investigated. A series of sulfonated polystyrene-*block*-polyethylene (PSS−PE) copolymers were synthesized to probe the interplay between crystallization, morphology, hydration, and proton transport. In block copolymer systems with amorphous hydrophobic blocks, it has been shown that higher water update and proton conductivity are obtained in low molecular weight systems. However, crystallization is known to disrupt the self-assembly of low molecular weight block copolymers. We found that this disruption results in lower water uptake and proton conductivity. Increasing molecular weight results in less morphological disruption and improvement in performance.

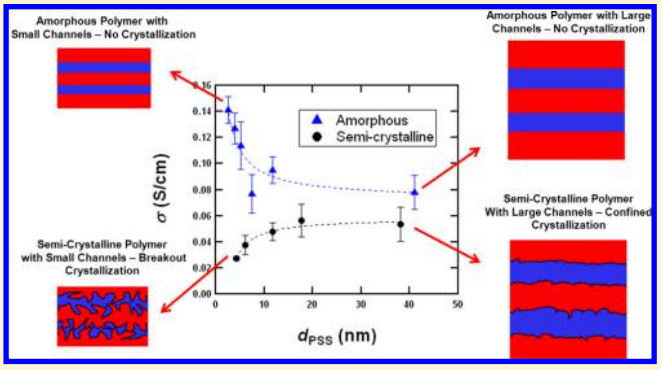

INTRODUCTION

Many high-volume commercial polymers such as polyethylene and polypropylene are semicrystalline. The crystalline regions in these polymers act as physical cross-links. Unlike chemical cross-links that are permanent, physical cross-links are reversible and therefore semicrystalline polymers are melt-processable when heated above the melting point of the crystallites. This paper is concerned with the characteristics of polymer electrolyte membranes (PEMs) used in applications such as fuel cells,[1] solar energy conversion devices,[2] and water filtration.[3] PEMs are polymers where a fraction of monomers are charged. One charge is bound to the backbone while the counterion is mobile. PEMs used for hydrogen fuel cells contain protons that are mobile in the hydrated state and serve to transport protons from anode to cathode. It is, perhaps, not surprising that the most commercially successful PEM, Nafion, is a semicrystalline polymer. Nafion is a random copolymer of hydrophobic tetrafluoroethylene and hydrophilic perfluoroether side chains that have terminal sulfonic acid groups. The excellent mechanical properties of Nafion are due to the semicrystalline nature of the hydrophobic backbone. There is limited, however, understanding of the interplay between the semicrystalline matrices and ion transport. The extent to which transport within hydrophilic domains in materials like Nafion is impeded in by the presence of a semicrystalline matrix is not known. The purpose of this paper is to present a series of model block copolymer PEMs that enables a systematic study of the relationship between polymer crystallization and ion transport.

This paper is part of a series on model PEMs based on diblock copolymers of sulfonated polystyrene and polyolefins.[4−9] The membranes used in this study contain nanometer sized domains with well-defined geometry that are charged and hydrophilic. Structural integrity of these membranes in the

Received: February 7, 2014
Revised: May 22, 2014
Published: June 19, 2014

hydrated state is governed by the polyolefin block (also referred to as the structural block). In a related study of sulfonated polystyrene-*block*-polymethylbutylene (PSS−PMB) copolymers, Park et al. found that decreasing the size of the conducting domains below 6 nm led to remarkable increases in proton conductivity and water uptake.[7] Possible reasons for this enhancement include elimination of ionic clusters due to confinement effects and a concomitant reduction in counterion condensation.[10,11] To achieve PEMs with small conducting domains, very low molecular weight PSS−PMB copolymers were required, and because PMB is a soft rubber, the resulting membranes had poor mechanical properties. One approach for improving the mechanical properties of such membranes is by physical-cross-linking due to crystallization of the hydrophobic block. In this article we focus on sulfonated polystyrene-*block*-polyethylene (PSS−PE) copolymers. These polymers are chemically similar to PSS−PMB. The only difference is the absence of the pendant methyl group in PE that makes the polymer semicrystalline. If the crystallites are confined within the PE domains, then one expects similar behavior from PSS−PMB and PSS−PE.

Confinement of crystalline domains within diblock copolymers wherein one of the blocks is amorphous (which we shall refer to as A−C block copolymer) has been studied extensively. A framework has been established to predict the self-assembly of copolymers with one nonconducting crystallizable block and one amorphous block.[12−21] The morphology obtained in these systems is dictated by the chemical incompatibility of the two blocks (χ, Flory−Huggins interaction parameter between A and C monomers) and the glass transition temperature, T_g, of the amorphous block.[12−21] When the amorphous block is glassy, the morphology of the melt state is retained and the crystallization of the second block is confined within the nanoscale domains.[14,16,19,22,23] However, our noncrystalline block must be rubbery to enable proton transport, and thus this mechanism of confinement is unimportant. When the amorphous block is rubbery, the morphology in the crystalline state depends on the segregation strength (χN, where N is the number of monomers per chain) between the blocks.[12,14,16,18] The melt-state morphology is retained only in strongly segregated systems when the product χN exceeds a certain critical value.[16−18] In weakly segregated systems, the crystalline phase "breaks out" of the confining block copolymer domain.[12−14,18,20,21] The morphology of the crystalline phase is often lamellar as this geometry is commensurate with that of chain folded crystals.[12,14,21,24,25] This was first anticipated by theorists[24,25] and subsequently observed experimentally.[12,14,21] The thermodynamic properties of our PSS-*b*-PE block copolymer are consistent with this general framework.

The desired trends in molecular weight for PEM performance and crystallization confinement are in direct conflict with each other. Our previous work on polymers with amorphous structural blocks indicates that conductivity is enhanced at low molecular weights while the literature indicates that confined crystallization is only expected in high molecular weight samples. The purpose of this paper is to elucidate this conflict.

MATERIALS AND METHODS

Sample Synthesis and Characterization. A poly(styrene-*block*-ethylene) (PS−PE) copolymer was synthesized by sequential anionic polymerization of styrene and butadiene, followed by selective hydrogenation of the polydiene as described previously.[26] Anionic polymerization was performed in cyclohexane to maximize the crystallinity of the PE block. Crystallinity of the PE block was confirmed using differential scanning calorimetry (DSC). Our samples exhibited between 24% and 28% crystallinity. Hydrogenation was followed by sulfonation of the PS block, as described by Park et al.,[7] to yield a sulfonated polystyrene-*block*-polyethylene (PSS−PE) block copolymer, the structure of which is shown in Figure 1. PSS−PE was

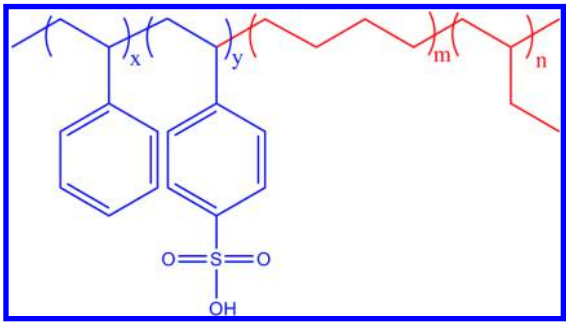

Figure 1. Chemical structure of sulfonated polystyrene-*block*-polyethylene (PSS−PE).

not soluble in dichloroethane at the reaction conditions used by Park et al.,[7] so a suspension of the PS−PE precursor was stirred vigorously under solvent reflux conditions to produce a more-or-less uniform dispersion of PS−PE which was then sulfonated under the same conditions described by Park et al.[7] While the extent of sulfonation was controlled, the locations of the sulfonic acid groups were not. The sulfonic acid groups are thus expected to be randomly distributed within the PSS block. The fraction of sulfonated styrene units, SL, as defined in eq 1, was determined using an ion exchange capacity measurement (IEC), which is quantified in eq 2 as the moles of sulfonic acid groups per gram of polymer (mmol/g).

$$\mathrm{SL} = \frac{\text{mol SSA}}{\text{mol S} + \text{mol SSA}} \tag{1}$$

$$\mathrm{IEC} = \frac{1000 \times \text{mol SSA}}{\mathrm{MW_{SSA}} \times \text{mol SSA} + \mathrm{MW_S} \times \text{mol S} + \mathrm{MW_E} \times \text{mol E}} \tag{2}$$

where SSA is styrenesulfonic acid, S is styrene, E is ethylene, and MW is molecular weight of the SSA, S, and E monomers in g/mol. The procedure for IEC measurement was taken from Zou et al.[27] Dried polymer of known mass was placed into a 0.1 M NaCl solution for 48 h to allow for the exchange of acidic protons on the PSS with sodium ions in solution. The concentration of protons was then determined by measuring the pH of the solution with a pH meter (Orion, Thermo Scientific). The IEC (mmequiv/g) was then determined using eq 3:

$$\mathrm{IEC} = \frac{\text{concentration of } \mathrm{H^+} \text{ in solution}}{\text{mass of dry polymer}} = \frac{10^{-\mathrm{pH}} \times V_{\mathrm{NaCl}}}{m_0} \times 1000 \tag{3}$$

where V_{NaCl} (L) is the volume of NaCl solution used and m_0 (kg) is the dry weight of the film. Measurements of SL and IEC were made at 25 °C. Previous work from our lab on PSS containing polymers has used NMR for determination of SL. The limited solubility of PSS−PE polymers in typical NMR solvents combined with the effect of changing molecular weight on polymer solubility made interpretation of NMR results challenging. The degree of hydration, λ, defined as the moles of water per mole of sulfonic acid groups in the membrane is calculated using eq 4:

$$\lambda = \frac{[\mathrm{H_2O}]}{[\mathrm{SO_3^-}]} = \frac{\mathrm{WU}\ (\%) \times 10}{\mathrm{MW_{H_2O}} \times \mathrm{IEC}\ (\mathrm{mmol/g})} \tag{4}$$

where $\mathrm{MW_{H_2O}}$ = 18.02 g/mol. The PE block is semicrystalline at this temperature.

dx.doi.org/10.1021/ma500298w | *Macromolecules* 2014, 47, 4330−4336

The characteristics of the polymers used in this study are summarized in Table 1. Determination of the volume fraction of the

Table 1. Characteristics of Polymers Used in This Study

sample ID[a]	PS MW (kg/mol)[b]	PSS MW (kg/mol)[c]	PE MW (kg/mol)[c]	ϕ_{PSS}[c]	IEC (mmol/g)[c]	SL[d]
p1	1.2	1.9	1.2	48	2.64	0.77
p3	2.5	3.9	2.2	51	2.67	0.74
p5	4.5	7.0	4.0	51	2.60	0.71
p9	9.0	14	7.7	52	2.73	0.74
p18	18	30	17	49	2.95	0.83

[a]Samples are labeled according to the nominal molecular weight of the non-sulfonated PS block. Sample p1, for example, is the PSS–PE block copolymer with a 1.2 kg/mol PS block. [b]Properties are of the PS–PE precursor. [c]Properties are of the PSS–PE sample studied. [d]SL calculated using eq 2

PSS phase was done using pure component densities (with S and E in the melt at 140 °C and assuming no effects due to mixing) with 0.97 (S),[26] 0.78 (E),[28] and 1.44 g/cm^3 (SSA).[6]

***In Situ* Small-Angle X-ray Scattering.** Samples for synchrotron small-angle X-ray scattering (SAXS) measurement were prepared by hot pressing at a temperature, T = 120 °C, to a thickness of 10 μm. SAXS was performed at beamline 7.3.3 at the Advanced Light Source (ALS) at Lawrence Berkeley National Laboratory[29] and at beamline 1-4 at the Stanford Synchrotron Radiation Laboratory (SSRL). Humidity-controlled SAXS was performed using a custom-designed humidity stage as reported previously.[30] Samples were equilibrated for 2 h at each relative humidity of interest before measurements were made. The original two-dimensional scattering images were azimuthally averaged to generate one-dimensional scattering intensity profiles, $I(q)$, where the magnitude of the scattering wave vector $q = 4\pi \sin(\theta/2)/\lambda$, where θ is scattering angle and λ is the wavelength of the incident beam.[31]

Water Uptake. Polymer films with thicknesses of about 200 μm were prepared by hot pressing at T = 120 °C. The films were dried in a vacuum oven at room temperature until the weight of the film was constant. The dry sample weights were measured immediately after they were removed from the vacuum oven. The dry film was placed in a quartz pan that was hooked on the end of a quartz spring (Deerslayer) in a humidity-controlled oven (SH-241, Espec. Corp). The spring and pan were held in a glass tube with an open end to avoid rotation and breakage due to the air flow. The spring extension was measured through an open window in the oven by a cathetometer equipped with an optical zoom telescope located outside the oven. Care was taken to minimize the time when the window was opened (typically 15 s). The spring was calibrated with standard masses at experimental temperatures and relative humidity in the chamber before use (spring constant was about 0.5 mN/mm). Water uptake, WU, is defined as the ratio of the weights of the sample after water uptake to that of the dry film weight, as shown in eq 5.

$$\mathrm{WU} = \frac{\text{hydrated film weight} - \text{dry film weight}}{\text{dry film weight}} \times 100\% \quad (5)$$

Conductivity. Free-standing films of PSS–PE with dimension 2 cm × 1 cm × 200 μm were prepared for conductivity measurements by hot pressing at T = 120 °C and then cutting to the appropriate shape using a razor blade. The thickness of sample films was measured using a micrometer. In-plane proton conductivity of hydrated membranes was measured by ac impedance spectroscopy using platinum electrodes in the standard four-probe configuration using a BekkTech sample clamp. Data were collected over a frequency range of 100 Hz–100 kHz in a humidity- and temperature-controlled oven (SH-241, Espec. Corp). Conductivity, σ, is given by

$$\sigma = \frac{l}{A \times R} \quad (6)$$

where A is the cross-sectional area of sample film, R is the touchdown of the Nyquist semicircle on the real axis, and l is the distance between the inner platinum electrodes.

RESULTS AND DISCUSSION

As discussed by Hamley et al.,[23] the stems of PE chains align roughly parallel to the interface between the two block copolymer phases when confined, while those of unconfined PE chains align orthogonal to the interface. The parallel orientation causes negligible changes in the interfacial area per chain, relative to the amorphous case, while the perpendicular orientation causes a decrease in interfacial area per chain. Changes in the interfacial area per chain result in a change in the domain size, d. As a result, when breakout occurs the domain size in the crystalline state, $d_c = 2\pi/q_c^*$, is larger than the domain size in the melt, $d_m = 2\pi/q_m^*$, while d_c is approximately equal to d_m when crystallization is confined.

Figure 2 shows SAXS profiles for dry polymer p1 in the crystalline state at T = 25 °C and in the melt at T = 120 °C.

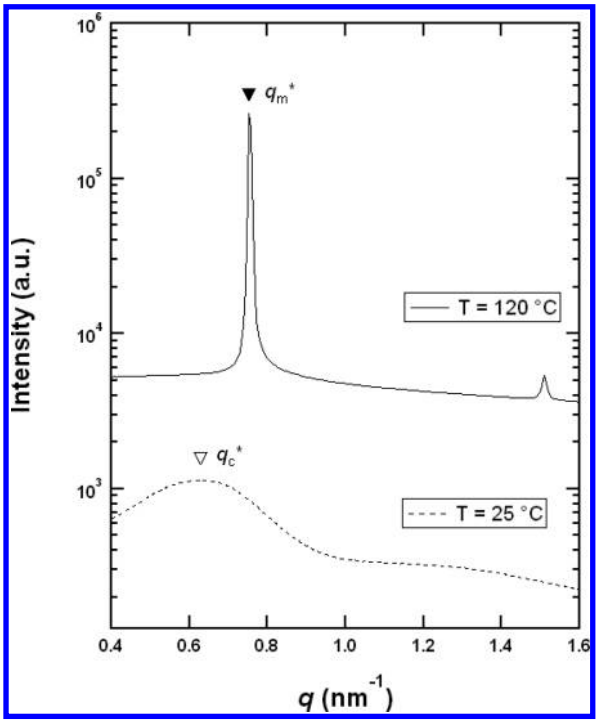

Figure 2. SAXS profiles of p1 in the crystalline state at T = 25 °C (bottom) and in the melt at T = 120 °C in the melt (top). The primary scattering peak in the crystalline state, q_c^*, is much smaller than primary scattering peak in the melt, q_m^*, indicating crystillazation increases the domain size, $d = 2\pi/q$, due to breakout of the PE crystallites.

The primary scattering peaks in the melt, q_m^*, and in the crystalline state, q_c^*, are indicated in the figure. The positions of q_m^* and q_c^* differ substantially, indicating that for p1 crystallization does affect the block copolymer self-assembly. SAXS profiles in the crystalline and melt states were obtained from all of the polymers listed in Table 1 in the dry state. Crystallization-induced disruption of domain structure, as measured by the ratio d_m/d_c, plotted as a function of MW_{PSS} in Figure 3, shows that the two smallest samples (p1 and p3) experience roughly comparable levels of disruption due to crystallization while the largest samples (p5, p9, and p18) experience no measurable level of disruption. Confined

dx.doi.org/10.1021/ma500298w | Macromolecules 2014, 47, 4330–4336

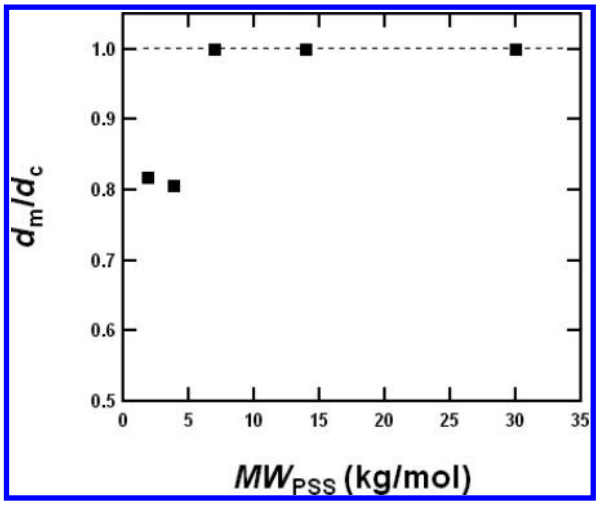

Figure 3. Effects of crystalline breakout on the domain size, d of PSS–PE, as measured by the ratio of the domain size in the melt, d_m, and the domain size in the crystalline state, d_c, plotted versus molecular weight of the PSS block.

crystallization is thus obtained in symmetric PSS–PE copolymers when MW_{PSS} exceeds 5 kg/mol.

Figure 4a shows *in situ* SAXS profiles of p1 for a variety of temperatures at RH = 95%. We focus on the position of the primary peak in the hydrated state, q_w*, of p1 which is a weak function of temperature. This indicates that the hydrated domain size, $d_w = 2\pi/q_w$*, is a weak function of temperature. This was true of all of the PSS–PE samples; the temperature dependence of d_w obtained from all samples is presented in Figure 4b. Dashed lines indicated the average of the values, which is effectively constant for all samples studied.

It has been shown previously that the effects of annealing in humid vapor can have an impact on PEM performance, specifically proton conductivity, σ.[9] This is particularly relevant for PSS–PE copolymers since proton conductivity of the benchmark for crystalline systems, Nafion is known to exhibit history-dependent behavior. It is unclear, however, if this behavior is due to the random copolymer architecture, semicrystalline backbone, or its high molecular weight. Figure 5 presents conductivity measurements obtained from two sequential heating scans from 25 to 90 °C and under constant controlled relative humidity, RH = 98%, for three different samples of p1. All three samples were prepared by the same protocol described above. In spite of this, conductivity measurements during the first heating scans differ significantly from each other. In contrast, conductivity measurements during the second heating scans from the three p1 samples are in reasonable agreement with each other. Figure 6 presents WU measurements obtained from two sequential heating scans from 25 to 90 °C and under constant controlled relative humidity, RH = 98%, for a single p1 sample. It was found that annealing samples at T = 90 °C and RH = 98% for 2 days led to reproducible data. The data reported below were obtained after this annealing protocol.

The effect of temperature on σ of PSS–PE exposed to air with RH = 98% is presented in Figure 7a. All samples showed Arrhenius-like behavior in σ, with values ranging from 2.8×10^{-2} to 5.6×10^{-2} S/cm at T = 25 °C and from 8.1×10^{-2} to 1.4×10^{-1} S/cm at T = 90 °C. Figure 7b shows the WU as a function of T at RH = 98%. WU is nearly independent of temperature for each copolymer.

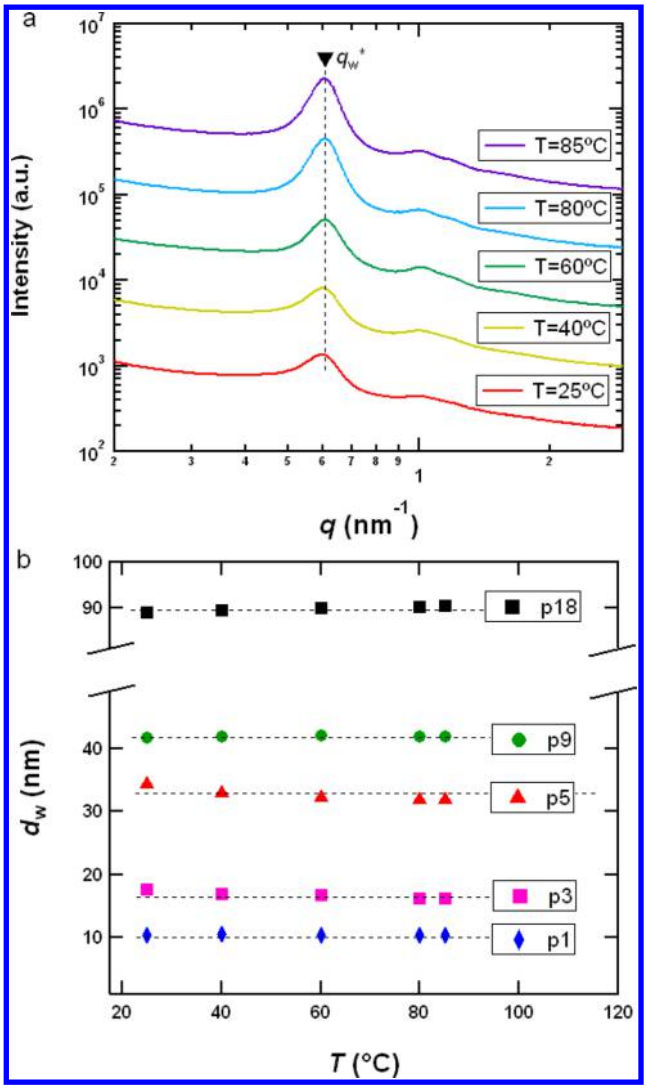

Figure 4. Small-angle X-ray scattering (SAXS) results for (a) p1 profiles at RH = 95% and T = 25, 40, 60, 80, and 85 °C (curves are vertically shifted with increasing T for visual clarity) and (b) hydrated domain sizes obtained from *in situ* SAXS as a function of hydrated domain size, d_w.

It is clear from Figure 7 that both σ and WU increase with increasing molecular weight. Increasing molecular weight results in an increase of the size of both the hydrophobic and hydrophilic domains. Since σ and WU relate primarily to the hydrophilic domains, we use the dry hydrophilic domain size, d_{PSS}, as the abscissa in the discussions that follow: $d_{PSS} = \phi_{PSS} d_c$ (all of the σ and WU measurements were made below the nominal PE melting temperature, and d_c is not affected by hydration).

The activation energy for proton transport, E_a, was obtained from Arrhenius fits of the temperature dependence of conductivity [$\sigma = \sigma_0 \exp(-E_a/RT)$, R is the universal gas constant] using the data presented in Figure 7a. In Figure 8, we plot E_a as a function of d_{PSS}. The activation energy appears to be independent of hydrophilic domain size, fluctuating around an average value of 14.5 kJ/mol. It is worth noting that this value is within error equal to the value observed in Nafion of 15 kJ/mol but larger than the expected value for a Grotthuss transport in pure water, 11 kJ/mol.[32] This suggests that proton

dx.doi.org/10.1021/ma500298w | *Macromolecules* 2014, 47, 4330–4336

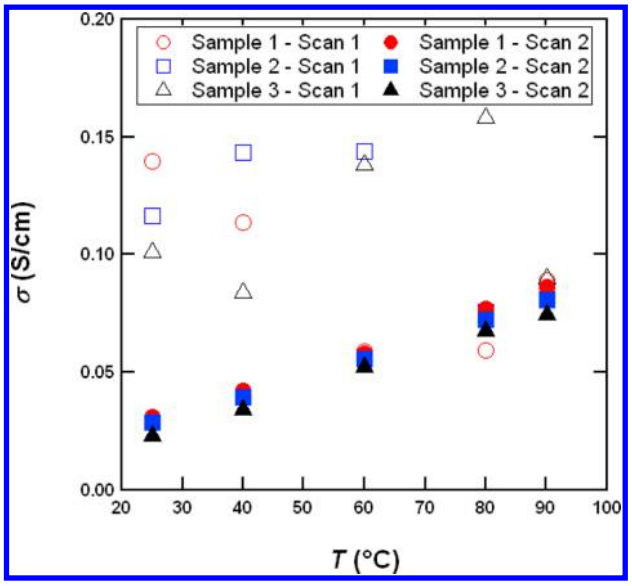

Figure 5. Effects of annealing on proton conductivity, σ, as a function of temperature, T, for p1 samples undergoing two sequential heating runs. Open symbols represent the first heating scan data, and closed symbols represent heating scan 2. Circles, squares, and triangles represent data from three independent samples. Data obtained during the second heating scan were taken as equilibrated values. Samples were tested in humid air at RH = 98%.

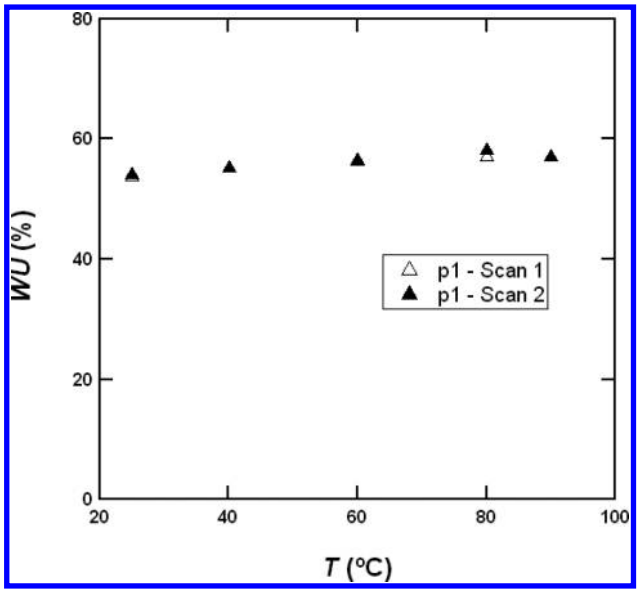

Figure 6. Effects of annealing on water uptake, WU, as a function of temperature, T. Open symbol represents the first heating scan (△), and closed symbols represent second heating scan (▲). Samples were tested in humid air at RH = 98%.

conduction is affected by confinement of nanoscale hydrophilic channels in a semicrystalline matrix.

In Figure 9a we show the effect of changing d_{PSS} on σ at T = 25 and 90 °C and RH = 98%. The dashed curves are fits to the functional form, $\sigma = kd_{PSS}^{m} + n$. This assumed functional form is purely empirical; we do not ascribe any significance to the fit parameters. Conductivity is found to increase with increasing domain size, reaching a plateau for samples p9 and p18. This trend is similar to that observed for d_m/d_c in Figure 2 and is consistent with the notion that disruption of the morphology

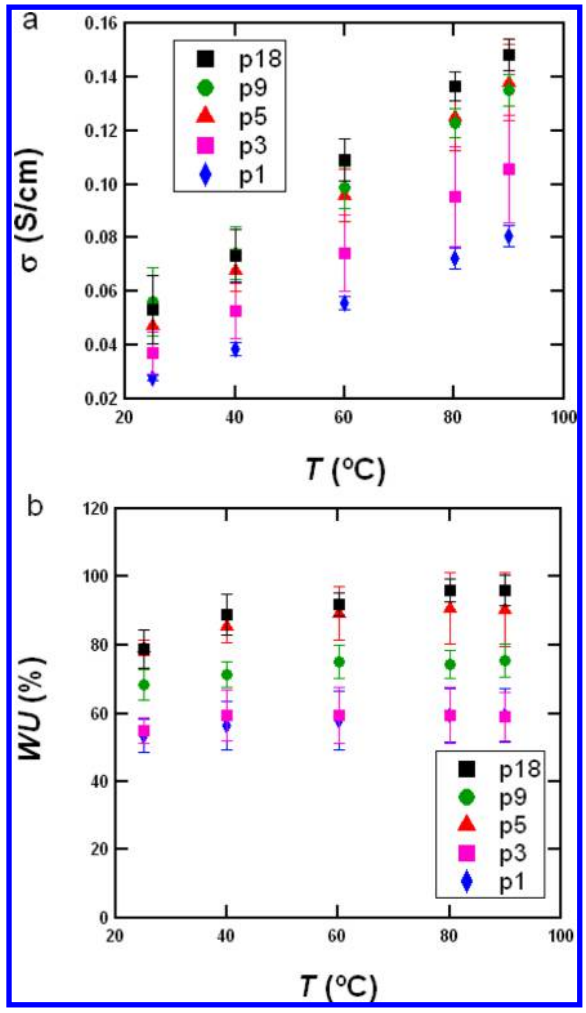

Figure 7. Temperature effects on (a) proton conductivity, σ, and (b) water uptake, WU. Samples were studied in humid air at RH = 98%.

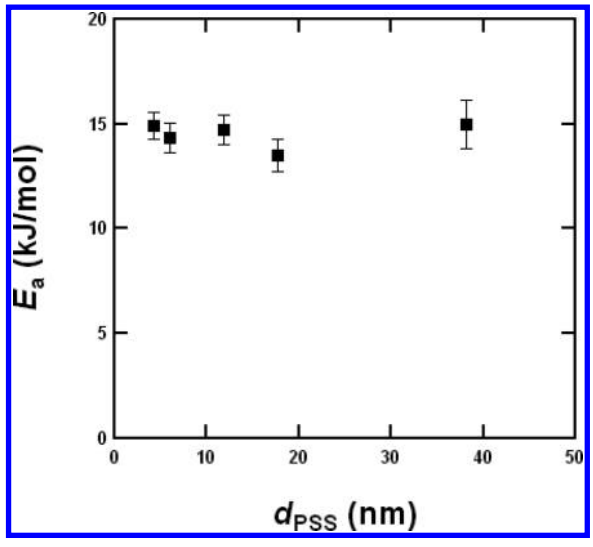

Figure 8. Activation energy, E_a, of proton transport as a function of PSS domain size, d_{PSS}, at RH = 98%.

due to breakout crystallization impedes proton transport in PEMs. A similar effect is seen in Figure 9b where WU is plotted as a function of d_{PSS}. Data presented are at T = 25 and 90 °C and RH = 98%. The dashed curves are fits to the functional

dx.doi.org/10.1021/ma500298w | Macromolecules 2014, 47, 4330−4336

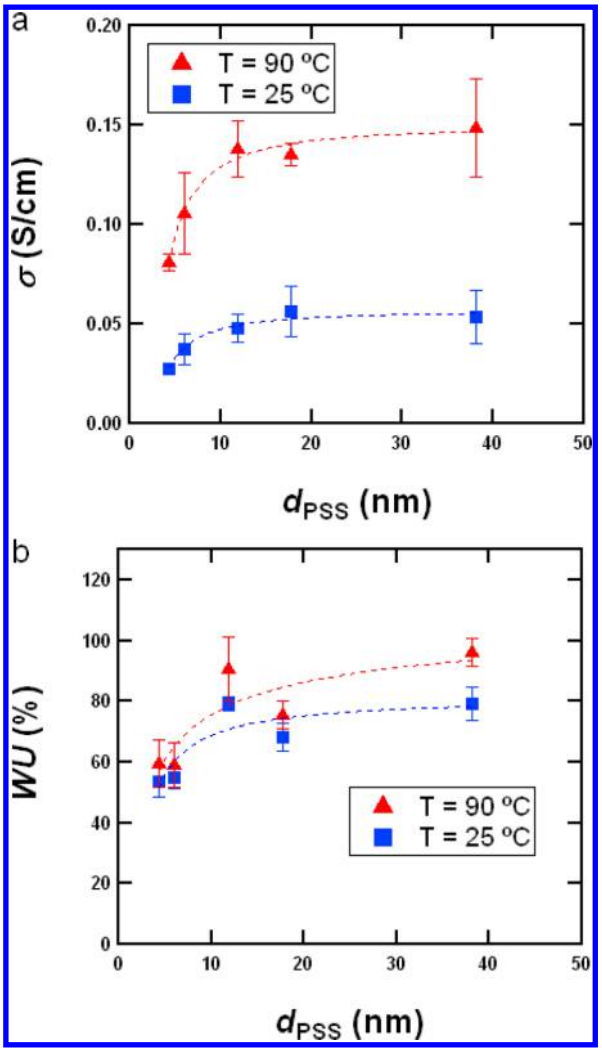

Figure 9. Effect of PSS domain size, d_{PSS}, on (a) proton conductivity, σ, at T = 25 (■) and 90 °C (▲) and (b) water uptake, WU, at T = 25 (■) and 90 °C (▲). Samples were equilibrated in air at RH = 98%.

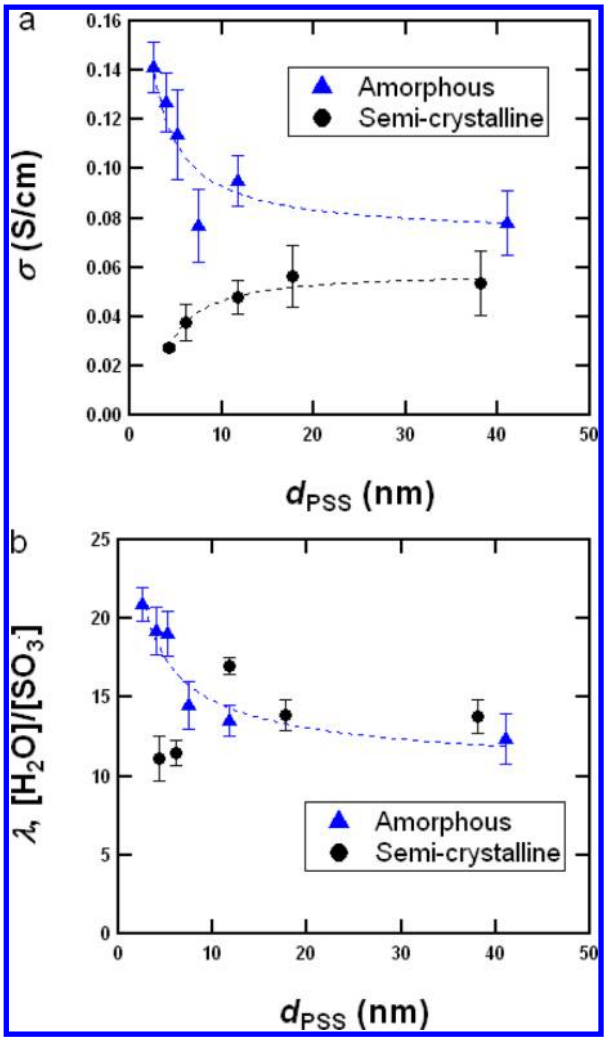

Figure 10. Comparison of amorphous and crystalline PSS block copolymers as a function of dry hydrophilic channel size at T = 25 °C for (a) proton conductivity and (b) water uptake. Samples were equilibrated in air at RH = 98%. Amorphous = PSS-PMB. Semi-crystalline = PSS-PE, the focus of this study.

form WU = $kd_{PSS}^{m} + n$. Breakout crystallization also reduces water uptake.

In Figure 10, we show the effect of changing d_{PSS} for the crystalline polymers of this study along with data from amorphous PSS−PMB samples studied by Park et al.[7] Data are presented for T = 25 °C and RH = 98% for brevity. Dashed lines represent power-law fits through the data ($\sigma = kd_{PSS}^{m} + n$). In Figure 10a, PSS−PMB with its amorphous structural block shows a decrease in σ with increasing d_{PSS}, while PSS−PE with its semicrystalline structural block shows an increase in σ with d_{PSS}. Despite their slight differences, these two systems converge to a nearly similar value of σ at high molecular weight. We attribute this to the suppression of breakout crystallization in PE phase at high molecular weights. The quantitative differences in the high molecular weight limit between the two systems in Figure 10a may be due to differences in IEC (in the case of the PSS−PMB study, the average IEC was 2.43 mmol/g while that for the PSS−PE was 2.72 mmol/g), or morphology (e.g. grain structure). In Figure 10b, we plot the hydration number λ versus d_{PSS} (we show λ instead of WU to provide a commonly used normalization based on IEC to account for slightly different ranges in IECs between the two systems). For the case of PSS−PMB λ decreases with increasing d_{PSS}. In contrast, λ increases with increasing d_{PSS} in the PSS−PE series. It is evident from Figure 10 that the nature of the structural block has a qualitative effect on proton transport in hydrated block copolymer membranes. These data combined with the data in Figure 3 suggest that confined crystallization in the structural block is important for maximizing proton transport in these systems.

■ CONCLUSION

We have studied morphology, water uptake, and proton conductivity of a series of symmetric PSS−PE copolymers with varying molecular weights equilibrated in humid air. The presence the semicrystalline PE block is found to perturb the self-assembly of the low molecular weight samples studied due to breakout crystallization. This effect leads to a reduction in both water uptake and proton conductivity. The observed trends in water uptake and conductivity are opposite of those observed in PSS−PMB block copolymers which contain an amorphous structural block. This study has shown that incorporation of a semicrystalline structural block is not an effective method for achieving mechanical stability in low molecular weight PEMs. While this conclusion may not apply

dx.doi.org/10.1021/ma500298w | Macromolecules 2014, 47, 4330−4336

to all PEMs, it certainly applies to PEMs composed of low molecular weight diblock copolymers. We speculate that further investigations into chemical cross-linking as studied by Chen et al.,[33] and more complex molecular architectures such as studied by Chen et al.,[34] are necessary to further understand how to achieve PEMs with all of the desired functionalities.

AUTHOR INFORMATION

Corresponding Author

*E-mail: nbalsara@berkeley.edu (N.P.B.).

Notes

The authors declare no competing financial interest.

ACKNOWLEDGMENTS

Primary funding for the work was provided by the Electron Microscopy of Soft Matter Program from the Office of Science, Office of Basic Energy Sciences, Materials Sciences and Engineering Division of the U.S. Department of Energy under Contract DE-AC02-05CH11231. SAXS experiments were performed at the Advanced Light Source (ALS) and the Stanford Synchrotron Radiation Laboratory (SSRL). The ALS is a DOE national user facility and is supported by the Director, Office of Science, Office of Basic Energy Sciences, of the U.S. Department of Energy under the same contract. SSRL is a Directorate of SLAC National Accelerator Laboratory and an Office of Science User Facility operated for the U.S. Department of Energy Office of Science by Stanford University. Certain commercial equipment, instruments, materials, suppliers and software are identified in this paper to foster understanding. Such identification does not imply recommendation or endorsement by the National Institute of Standards and Technology, nor does it imply that the materials or equipment identified are necessarily the best available for the purpose.

REFERENCES

(1) Kreuer, K. D. *J. Membr. Sci.* **2001**, *185* (1), 29−39.
(2) Li, B.; Wang, L. D.; Kang, B. N.; Wang, P.; Qiu, Y. *Sol. Energy Mater. Sol. Cells* **2006**, *90* (5), 549−573.
(3) Geise, G. M.; Freeman, B. D.; Paul, D. R. *Polymer* **2010**, *51* (24), 5815−5822.
(4) Beers, K. M.; Yakovlev, S.; Jackson, A. J.; Wang, X.; Hexemer, A.; Downing, K. H.; Balsara, N. P. *J. Phys. Chem. B* **2014**, *118*, 6785−6791.
(5) Park, M. J.; Balsara, N. P. *Macromolecules* **2008**, *41* (10), 3678−3687.
(6) Park, M. J.; Balsara, N. P.; Jackson, A. *Macromolecules* **2009**, *42* (17), 6808−6815.
(7) Park, M. J.; Downing, K. H.; Jackson, A.; Gomez, E. D.; Minor, A. M.; Cookson, D.; Weber, A. Z.; Balsara, N. P. *Nano Lett.* **2007**, *7* (11), 3547−3552.
(8) Park, M. J.; Nedoma, A. J.; Geissler, P. L.; Balsara, N. P.; Jackson, A.; Cookson, D. *Macromolecules* **2008**, *41* (6), 2271−2277.
(9) Wang, X.; Yakovlev, S.; Beers, K. M.; Park, M. J.; Mullin, S. A.; Downing, K. H.; Balsara, N. N. *Macromolecules* **2010**, *43* (12), 5306−5314.
(10) Balsara, N. P.; Beers, K. M. *Eur. Polym. J.* **2011**, *47* (4), 647−650.
(11) Beers, K. M.; Balsara, N. P. *ACS Macro Lett.* **2012**, 1155−1160.
(12) Rangarajan, P.; Register, R. A.; Fetters, L. J.; Bras, W.; Naylor, S.; Ryan, A. J. *Macromolecules* **1995**, *28* (14), 4932−4938.
(13) Ryan, A. J.; Hamley, I. W.; Bras, W.; Bates, F. S. *Macromolecules* **1995**, *28* (11), 3860−3868.
(14) Quiram, D. J.; Register, R. A.; Marchand, G. R. *Macromolecules* **1997**, *30* (16), 4551−4558.
(15) Hamley, I. W. *Adv. Polym. Sci.* **1999**, *148*, 113−137.
(16) Loo, Y. L.; Register, R. A.; Ryan, A. J. *Phys. Rev. Lett.* **2000**, *84* (18), 4120−4123.
(17) Loo, Y. L.; Register, R. A.; Ryan, A. J.; Dee, G. T. *Macromolecules* **2001**, *34* (26), 8968−8977.
(18) Loo, Y. L.; Register, R. A.; Ryan, A. J. *Macromolecules* **2002**, *35* (6), 2365−2374.
(19) Zhu, L.; Cheng, S. Z. D.; Calhoun, B. H.; Ge, Q.; Quirk, R. P.; Thomas, E. L.; Hsiao, B. S.; Yeh, F.; Lotz, B. *Polymer* **2001**, *42* (13), 5829−5839.
(20) Xu, J. T.; Fairclough, J. P. A.; Mai, S. M.; Chaibundit, C.; Mingvanish, M.; Booth, C.; Ryan, A. J. *Polymer* **2003**, *44* (22), 6843−6850.
(21) Mai, S. M.; Fairclough, J. P. A.; Viras, K.; Gorry, P. A.; Hamley, I. W.; Ryan, A. J.; Booth, C. *Macromolecules* **1997**, *30* (26), 8392−8400.
(22) Loo, Y. L.; Register, R.; Ryan, A. *Abstr. Pap. Am. Chem. Soc.* **1999**, *218*, U672−U672.
(23) Hamley, I. W.; Fairclough, J. P. A.; Bates, F. S.; Ryan, A. J. *Polymer* **1998**, *39* (6−7), 1429−1437.
(24) Dimarzio, E. A.; Guttman, C. M.; Hoffman, J. D. *Macromolecules* **1980**, *13* (5), 1194−1198.
(25) Whitmore, M. D.; Noolandi, J. *Macromolecules* **1988**, *21* (5), 1482−1496.
(26) Wong, D. T.; Mullin, S. A.; Battaglia, V. S.; Balsara, N. P. *J. Membr. Sci.* **2012**, *394*, 175−183.
(27) Zou, L.; Roddecha, S.; Anthamatten, M. *Polymer* **2009**, *50* (14), 3136−3144.
(28) Fetters, L. J.; Lohse, D. J.; Richter, D.; Witten, T. A.; Zirkel, A. *Macromolecules* **1994**, *27* (17), 4639−4647.
(29) Hexemer, A.; Bras, W.; Glossinger, J.; Schaible, E.; Gann, E.; Kirian, R.; MacDowell, A.; Church, M.; Rude, B.; Padmore, H. *J. Phys., Conf. Ser.* **2010**, *247*, 012007 (11 pp.)−012007 (11 pp.)012007 (11 pp.).
(30) Jackson, A.; Beers, K. M.; Chen, X. C.; Hexemer, A.; Pople, J. A.; Kerr, J. B.; Balsara, N. P. *Rev. Sci. Instrum.* **2013**, *84* (7), 075114.
(31) Ilavsky, J. *J. Appl. Crystallogr.* **2012**, *45* (2), 324−328.
(32) Weber, A. Z.; Newman, J. *J. Electrochem. Soc.* **2004**, *151* (2), A311−A325.
(33) Chen, L.; Hallinan, D. T., Jr.; Elabd, Y. A.; Hillmyer, M. A. *Macromolecules* **2009**, *42* (16), 6075−6085.
(34) Chen, Y. B.; Thorn, M.; Christensen, S.; Versek, C.; Poe, A.; Hayward, R. C.; Tuominen, M. T.; Thayumanavan, S. *Nat. Chem.* **2010**, *2* (6), 503−508.